

# Evidence of a higher nodal band $\alpha+^{44}\text{Ca}$ cluster state in fusion reactions and $\alpha$ clustering in $^{48}\text{Ti}$

S. Ohkubo<sup>1</sup>

<sup>1</sup>*Research Center for Nuclear Physics, Osaka University, Ibaraki, Osaka 567-0047, Japan*  
(Dated: February 11, 2022)

In the nucleus  $^{48}\text{Ti}$ , whose structure is essential in evaluating the half-life of the neutrinoless double- $\beta$  decay ( $0\nu\beta\beta$ ) of  $^{48}\text{Ca}$ , the existence of the  $\alpha$  cluster structure is shown for the first time. A unified description of scattering and structure is performed for the  $\alpha + ^{44}\text{Ca}$  system. By using a global potential, which reproduces experimental  $\alpha + ^{44}\text{Ca}$  scattering over a wide range of incident energies,  $E_\alpha=18 - 100$  MeV, it is shown that the observed  $\alpha + ^{44}\text{Ca}$  fusion excitation function at  $E_\alpha=9 - 18$  MeV is described well. The bump at  $E_\alpha=10.2$  MeV is found to be due to a resonance which is a  $7^-$  state of the higher nodal band with the  $\alpha + ^{44}\text{Ca}$  cluster structure in  $^{48}\text{Ti}$ . The local potential  $\alpha + ^{44}\text{Ca}$  cluster model locates the ground band of  $^{48}\text{Ti}$  in agreement with experiment and reproduces the enhanced  $B(E2)$  values in the ground band well. This shows that collectivity due to  $\alpha$  clustering in  $^{48}\text{Ti}$  should be taken into account in the evaluation of the nuclear matrix element in the  $0\nu\beta\beta$  double- $\beta$  decay of  $^{48}\text{Ca}$ .

## I. INTRODUCTION

$\alpha$  clustering is essential not only in the light  $0p$ -shell and  $sd$  shell regions [1, 2] but also in the medium-weight  $fp$  shell region [3, 4] as evidenced typically in the  $^{44}\text{Ti}$  region [5–14]. Recent evidence of the higher nodal band states with the  $\alpha$  cluster structure in  $^{52}\text{Ti}$  [15], in which the intercluster relative motion is excited, suggests that  $\alpha$  clustering may persist in nuclei in-between such as  $^{48}\text{Ti}$  and  $^{46}\text{Ti}$ . In fact, the  $\alpha$  spectroscopic factors of  $^{48}\text{Ti}$  and  $^{46}\text{Ti}$  in the  $(^6\text{Li}, d)$   $\alpha$ -transfer reactions [16, 17] are larger than that of  $^{52}\text{Ti}$ , which is the minimum in the  $A=36\text{--}64$  mass region [16]. This is also confirmed in the  $(p, p\alpha)$  reactions [18–20]. Reference [21] reports that the excess neutrons outside the core work as covalent bonding between the clusters.

The structure of  $^{48}\text{Ti}$  is crucial in determining the nature of neutrino, Dirac or Majorana particle in the measurements of neutrinoless double- $\beta$  decay  $0\nu\beta\beta$  of  $^{48}\text{Ca}$  [22]. The study of  $0\nu\beta\beta$  [23], which violates lepton number conservation, serves to solve the longstanding fundamental questions beyond the standard model. The inverse half-life of  $0\nu\beta\beta$  of  $^{48}\text{Ca}(0^+) \rightarrow ^{48}\text{Ti}(0^+)$  is given by  $[T_{1/2}^{0\nu}]^{-1} = G_{0\nu} |< m_{\beta\beta} > / m_e|^2 |M^{0\nu}|^2$ , where  $< m_{\beta\beta} >$  is the effective Majorana neutrino mass,  $m_e$  is the electron mass, and  $G_{0\nu} \sim 10^{-14} \text{ yr}^{-1}$  is a phase-space factor. For the evaluation of the nuclear matrix element of the transition  $M^{0\nu}$  [24], it is essential to know the ground state wave function of  $^{48}\text{Ti}$  accurately.

Several approaches such as the shell model [25–28], ab initio calculations [29, 30], quasi-particle random phase approximation [31–33], the projected Hartree-Fock Bogoliubov model [34], the generator coordinate method (GCM) [35, 36], the energy density functional [37, 38] and the interacting boson model [39] have been reported. As for the  $\alpha$  clustering aspects of  $^{48}\text{Ti}$ , a microscopic  $\alpha + ^{44}\text{Ca}$  cluster model calculation in the GCM was performed [40, 41]. However, no state corresponding to the ground state of  $^{48}\text{Ti}$  was obtained. Experimentally in

the recent challenges [42, 43], no  $\alpha$  cluster states have been observed in  $^{48}\text{Ti}$ . A discovery of a typical  $\alpha$  cluster state, such as the higher nodal band states observed in  $^{52}\text{Ti}$  [15], would shed light on the  $\alpha$  clustering of the ground state of  $^{48}\text{Ti}$ .

The purpose of this paper is to show that the existence of a higher nodal band  $\alpha + ^{44}\text{Ca}$  cluster structure in  $^{48}\text{Ti}$  is evidenced for the first time by investigating the observed  $\alpha + ^{44}\text{Ca}$  fusion cross sections with a global Luneburg lens-like [44–46] potential that describes  $\alpha + ^{44}\text{Ca}$  scattering over a wide range of incident energies,  $E_\alpha=18 - 100$  MeV. By using the local potential  $\alpha + ^{44}\text{Ca}$  cluster model the observed enhanced  $B(E2)$  values of the ground band of  $^{48}\text{Ti}$  are reproduced well. It is shown that the enhanced  $B(E2)$  values are caused by  $\alpha$  clustering in  $^{48}\text{Ti}$ .

The paper is organized as follows. Section II is devoted to the analysis of  $\alpha + ^{44}\text{Ca}$  scattering and fusion reactions using a global potential. In Sec. III  $\alpha + ^{44}\text{Ca}$  cluster structure in  $^{48}\text{Ti}$  is studied. In Sec. IV discussions and a summary are given.

## II. ANALYSIS OF $\alpha + ^{44}\text{Ca}$ SCATTERING AND FUSION REACTIONS

In exploring the  $\alpha$  cluster structure in medium-weight mass region where the level density is high, a unified description of  $\alpha$  scattering including rainbow scattering, prerainbows, backward angle anomaly (BAA) or anomalous large angle scattering and the  $\alpha$  cluster structure in the bound and quasi-bound energy region has been very powerful [4–7, 13, 15]. In fact, the  $\alpha$  cluster structure in the  $^{44}\text{Ti}$  region was successfully explored from this viewpoint and the predicted  $\alpha$  cluster  $K = 0^-$  band with the  $\alpha + ^{40}\text{Ca}$  cluster structure [5–7], which is a parity-doublet partner of the ground band of  $^{44}\text{Ti}$ , was observed in experiment [8, 9]. Systematic theoretical and experimental studies in the  $^{44}\text{Ti}$  region [3, 10–14] confirmed the existence of the  $\alpha$  cluster in the beginning of the  $fp$ -shell.

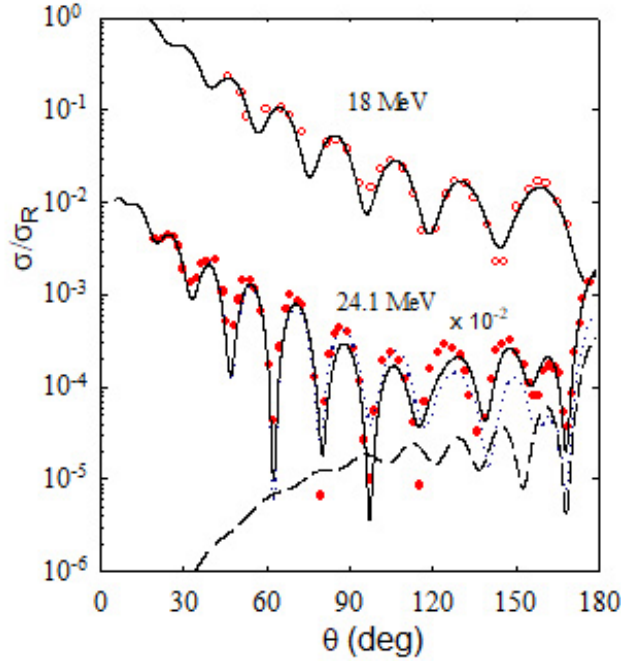


FIG. 1. (Color online) Angular distributions in  $\alpha+^{44}\text{Ca}$  scattering at  $E_\alpha=18$  and 24.1 MeV calculated with the optical potentials in Table I (solid lines) are compared with the experimental data (circles) [49]. The calculated angular distributions are decomposed into the barrier-wave (dotted lines) and the internal-wave (dashed lines) contributions. At 18 MeV the solid line overlaps with the dotted line and the dashed line is negligibly small and is not drawn.

TABLE I. The optical potential parameters used in Fig. 1 and the volume integrals per nucleon pair,  $J_v$ , in unit of  $\text{MeVfm}^3$  for the real potentials.  $E_\alpha$ ,  $V$ ,  $W$  and  $W_s$  are in units of MeV and  $r_v$ ,  $a_v$ ,  $r_w$ ,  $a_w$ ,  $r_s$  and  $a_s$  are in units of femtometers.

$E_\alpha$	$J_v$	$V$	$r_v$	$a_v$	$W$	$r_w$	$a_w$	$W_s$	$r_s$	$a_s$
18	388	181	1.42	1.25	14.0	1.75	0.934	53.2	1.36	0.378
24.1	356	166	1.42	1.25	10.6	1.75	0.934	17.0	1.36	0.378

The BAA in  $\alpha$  particle scattering, which was first observed for  $\alpha+^{40}\text{Ca}$  [47, 48], was systematically investigated in comparison with the isotopes  $^{42}\text{Ca}$  and  $^{44}\text{Ca}$  [49] at low energies,  $E_\alpha=18\text{--}29$  MeV. It was concluded [49] that  $\alpha+^{44}\text{Ca}$  scattering with no backward enhancement, which is described well by the so-called standard optical with a Wood-Saxon form factor, is normal. The normal behavior of the angular distributions was attributed to strong absorption due to the excess neutrons outside the  $^{40}\text{Ca}$  core [40, 41, 49, 50] and little attention has been paid to the  $\alpha+^{44}\text{Ca}$  cluster structure of  $^{48}\text{Ti}$  in contrast to the  $\alpha+^{40}\text{Ca}$  cluster structure in  $^{44}\text{Ti}$ .

I extend the global optical potential determined in  $\alpha+^{44}\text{Ca}$  scattering over a wide range of energies of  $E_\alpha=24\text{--}100$  MeV [50] to the lower energies  $E_\alpha=9\text{--}24$  MeV. The optical potentials are given by

$U(r) = -Vf^2(r; R_v, a_v) + V_{Coul}(r) - iWf^2(r; R_w, a_w) - i4a_sW_s\frac{d}{dr}f^2(r; R_s, a_s)$  with  $f(r; R_i, a_i) = 1/\{1 + \exp[(r - R_i)/a_i]\}$ . The Coulomb potential is assumed to be a uniformly charged sphere with a reduced radius  $r_c=1.3$  fm. First, I show that the experimental angular distribution in  $\alpha+^{44}\text{Ca}$  scattering at the lowest energy  $E_\alpha=18$  MeV is reproduced well by the global potential. In Fig. 1 the calculated angular distributions at 18 MeV and 24.1 MeV are compared with the experimental data. The potential parameters  $V$ ,  $W$  and  $W_s$  are searched with other parameters fixed as in Ref. [50], which are listed in Table I. The fits to the experimental data are much better than the ones calculated with the standard optical model in Ref. [49] and the improvements are entirely due to the Luneburg lens-like shape of the real potential [44–46]. To see why BAA of the cross sections is absent, the calculated angular distributions are decomposed using the technique of Ref.[51] into the barrier-wave component reflected at the surface and the internal-wave component, which penetrates deep into the internal region of the potential [52]. In Fig. 1, the barrier-waves dominate and the internal-waves hardly contribute, not visible at 18 MeV. The absence of the BAA in  $\alpha+^{44}\text{Ca}$  scattering is due to no internal-wave contributions under strong absorption, and not due to the real part of the potential since it is similar to the  $\alpha+^{40}\text{Ca}$  system as will be shown in Fig. 6.

Second, I investigate the  $\alpha+^{44}\text{Ca}$  fusion cross sections below  $E_\alpha=18$  MeV. In contrast to  $\alpha+^{40}\text{Ca}$  [5, 53–55], the  $\alpha+^{44}\text{Ca}$  fusion excitation function with no pronounced oscillations [54] has never been paid attention to in the past decades. However, one note in Fig. 2 that the observed excitation function is not monotonic with a bump at around  $E_\alpha=10.2$  MeV where absorption is relatively small near the threshold. The origin of this bump, which may be a remnant of the fusion oscillations seen typically for  $\alpha+^{40}\text{Ca}$  [53–55],  $^{12}\text{C}+^{12}\text{C}$  [56],  $^{16}\text{O}+^{12}\text{C}$  and  $^{16}\text{O}+^{16}\text{O}$  [57], seems to be related to the  $\alpha+^{44}\text{Ca}$  molecular resonance.

In calculating the fusion cross sections using the optical potential, I followed the prescription used for  $\alpha+^{40}\text{Ca}$  in Ref.[53] where the fusion cross section is defined as a total reaction cross section due to the short-ranged imaginary potential. The fusion cross sections at  $E_\alpha < 18$  MeV are calculated using the optical potential at  $E_\alpha=18$  MeV in Table I with  $r_w=1.3$  for the volume imaginary potential and  $W_s=0$  for the surface imaginary potential due to direct reactions. The energy dependence of the strength parameter,  $W$ , which was originally determined at  $E_\alpha > 24$  MeV in Ref. [50] is modified for  $E_\alpha < 18$  MeV to decrease linearly toward the barrier top energy due to the dispersion relation of the threshold anomaly [58],  $W=aE_\alpha + b$  for  $E_\alpha \geq 8.4$  MeV with  $a=1.281$  and  $b=-10.74$ .

In Fig. 2 the calculated fusion excitation function is compared with the experimental data [54]. It is to be noted that the bump at  $E_\alpha=10.2$  MeV, which was not reproduced in Ref. [54], is reproduced well by the cal-

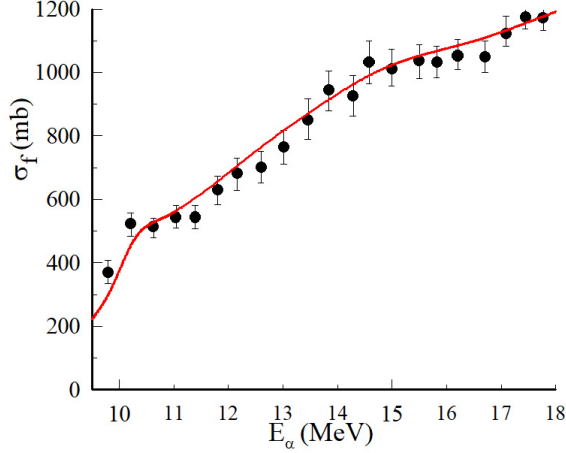


FIG. 2. (Color online) Calculated excitation function of the  $\alpha + {}^{44}\text{Ca}$  fusion cross sections (solid lines) is compared with the experimental data (filled circles) [54].

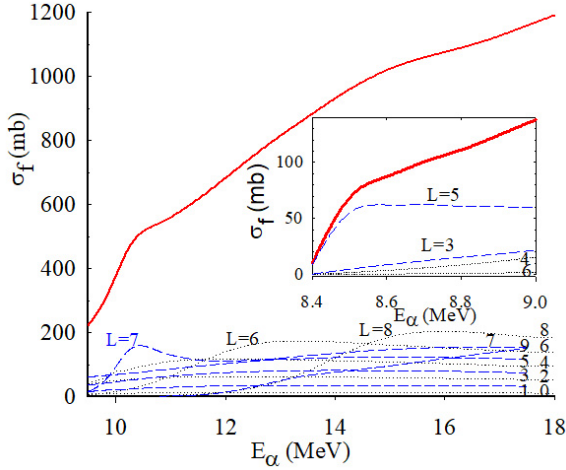


FIG. 3. (Color online) Calculated excitation functions of the  $\alpha + {}^{44}\text{Ca}$  fusion cross sections (solid lines) are decomposed into the partial wave contributions; even  $L$  (dotted lines) and odd  $L$  (dashed lines). The inset is for  $E_\alpha = 8.4\text{--}9.0$  MeV.

culuation. Also the calculated fusion cross sections do not decrease monotonically toward the threshold energy in accordance with the very smooth oscillatory behavior of the experimental data, which is a remnant of the pronounced oscillatory structure seen in the fusion excitation function for  $\alpha + {}^{40}\text{Ca}$  in the same energy region. The emergence of a bump at  $E_\alpha = 10.2$  MeV is due to the relatively weak absorption near the barrier top energy,  $E = 6.2$  MeV, which corresponds to  $E_\alpha = 7.2$  MeV.

In Fig. 3 the calculated fusion cross sections are decomposed into the partial cross sections. One notes that the bump peak is caused by the partial fusion cross sections with  $L=7$  (dashed line). The broad resonance-like behavior of the  $L=6$  and  $8$  partial fusion cross sections contributes to the non-monotonic behavior of the fusion ex-

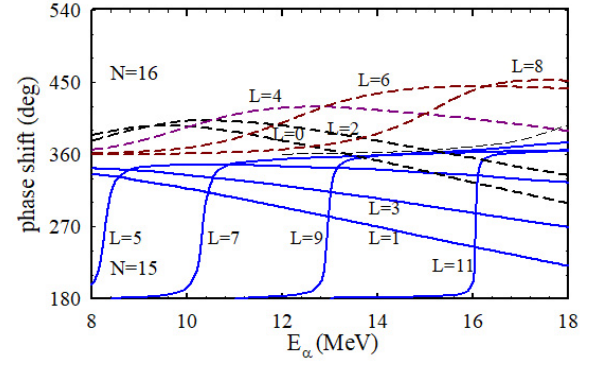


FIG. 4. (Color online) The phase shifts for  $\alpha + {}^{44}\text{Ca}$  scattering calculated with the D181 real potential. The vertical axis is  $\delta_L - m_L\pi$  where  $m_L$  is the number of the Pauli-forbidden states. See the text. The resonances for odd  $L$  and even  $L$  correspond to  $N = 15$  and  $N = 16$ , respectively.

citation function. The calculated fusion excitation function at  $E_\alpha = 8.4\text{--}9$  MeV is displayed in the inset. Although the magnitude of the cross sections becomes smaller, one notices the appearance of a bump at  $E_\alpha = 8.5\text{--}8.6$  MeV where the absorption is much smaller than the bump at  $E_\alpha = 10.2$  MeV. It is found that this structure is caused by the  $L=5$  partial cross sections (dashed line).

In order to reveal the origin of the bump structures in the fusion excitation function, in Fig. 4 the phase shifts calculated with  $V = 181$  MeV potential (referred to as D181 hereafter) at  $E_\alpha = 18$  MeV by switching off the imaginary potentials are displayed. One notes that the resonance at  $E_\alpha = 10.3$  MeV with a width  $\Gamma_{c.m.} = 0.18$  MeV is responsible for the peak of the partial fusion cross section for  $L = 7$  and therefore for the bump observed at around  $E_\alpha = 10.2$  MeV. The resonance at  $E_\alpha = 8.3$  MeV with  $\Gamma_{c.m.} = 0.22$  MeV is also responsible for the bump at  $E_\alpha = 8.3$  MeV in the inset of Fig. 3. There appear resonances for  $L = 9$  and  $11$  at  $E_\alpha = 12.96$  ( $\Gamma_{c.m.} = 0.11$  MeV) and  $16.07$  ( $\Gamma_{c.m.} = 0.04$  MeV), respectively, however, the contributions to the fusion cross section are not seen clearly. The broad  $L = 6$  and  $8$  resonances at around  $E_\alpha = 12$  MeV and  $16$  MeV, respectively, are also the origin of the non-monotonic behavior of the fusion excitation function.

### III. $\alpha + {}^{44}\text{Ca}$ CLUSTER STRUCTURE IN ${}^{48}\text{Ti}$

How these resonances are understood as the highly excited states with the  $\alpha + {}^{44}\text{Ca}$  cluster structure in  ${}^{48}\text{Ti}$ ? In Fig. 5(a) the energy levels calculated with the D181 potential is displayed. The number of the Pauli-forbidden redundant states in the  $\alpha + {}^{44}\text{Ca}$  cluster model [40] is  $m_L = (12 - L)/2$  for even  $L \leq 12$  and  $m_L = (13 - L)/2$  for odd  $L \leq 13$ .  $m_L = 0$  for  $L \geq 14$ . According to the generalized Levinson theorem [59], the phase shift  $\delta_L$  in which the existence of the Pauli-forbidden states are taken into account should satisfy  $\delta_L = m_L\pi$  at  $E_\alpha = 0$

TABLE II. Calculated intercluster rms radii (femtometers) and  $B(E2)$  values (W.u.) for the  $J \rightarrow (J-2)$  transitions of the ground band of  $^{48}\text{Ti}$ . The  $B(E2)$  values calculated with the D171 potential (cal-1) and the  $L$ -dependent  $V$  (MeV) (cal-2) are compared with the experimental data [72].

$J^\pi$	$\langle R^2 \rangle^{1/2}$	$B(E2)$		$V$		$B(E2)$
		cal-1	cal-1 exp.[72]	cal-2	cal-2	
$0^+$	4.41			171.0		
$2^+$	4.37	13.6	15.0	169.4	13.8	
$4^+$	4.33	17.9	18.4	167.7	18.8	

and tends asymptotically to  $\delta_L = 0$  at  $E_\alpha = \infty$ . Shown in Fig. 4 are the phase shifts,  $\delta_L - m_L \pi$ , to make easy to see the band structure of  $N = 15$  and  $N = 16$  where  $N = 2n + L$  with  $n$  being the number of nodes in the relative wave function with the  $\alpha + ^{44}\text{Ca}$  molecular structure. Surprisingly the calculated lowest Pauli-allowed  $N = 12$  band, which satisfies the Wildermuth condition due to the Pauli principle, falls in correspondence to the experimental ground band of  $^{48}\text{Ti}$ . One finds that the  $L = 7$  resonance that contributes to the bump of the fusion cross section at  $E_\alpha = 10.2$  MeV is a member state of the higher nodal  $N = 15$  band with the  $\alpha + ^{44}\text{Ca}$  cluster structure, in which the intercluster relative motion is one more excited compared with the  $N = 13$  band. This  $7^-$  of  $N = 15$  is a second example of the higher nodal band with negative parity in addition to  $^{44}\text{Ti}$  [12, 13], which gives strong support to the persistence of the  $\alpha$  cluster structures in  $^{48}\text{Ti}$ . It is highly desired to observe the  $5^-$  state theoretically predicted at  $E_\alpha = 8.3$  MeV as well as the  $3^-$  and  $1^-$  states of the  $N = 15$  band in a precise experiment such as sub-barrier fusion reactions [60, 61] and transfer reactions etc., although the  $\alpha$ -strengths as well as the  $N = 13$  and 14 bands, may be fragmented as in  $^{40}\text{Ca}$  and  $^{44}\text{Ti}$  [10–13].

The reason why the  $7^-$  state of  $N = 15$  is observed in Fig. 2 is related to the considerably high  $\alpha$  threshold energy of  $^{48}\text{Ti}$ , 9.45 MeV due to a non- $\alpha$  nucleus. Because of this, although the excitation energy  $E_x = 18.8$  MeV of the  $7^-$  state is high, the energy from the  $\alpha$  threshold becomes relatively small. The  $N = 14$  band, which is a higher nodal band of the ground band  $N = 12$ , starts just above the  $\alpha$  threshold. Its observation in addition to the known analog higher nodal bands in  $^{20}\text{Ne}$  [62–65],  $^{40}\text{Ca}$  [10, 11],  $^{44}\text{Ti}$  [10, 12, 13] and  $^{52}\text{Ti}$  [15, 43] would also reinforce the  $\alpha$  cluster structure in  $^{48}\text{Ti}$ .

As for the  $N = 12$  ground band, the D181 potential with  $J_v = 388$  MeVfm<sup>3</sup> determined at  $E_\alpha = 18$  MeV locates the ground state  $0^+$ , which overbinds -4.27 MeV, compared with the experimental ground state. When discussing the ground band deep below the threshold, as was the case in  $^{52}\text{Ti}$  [15], the potential must be readjusted by taking into account that the volume integral of the real potential decreases toward the threshold due

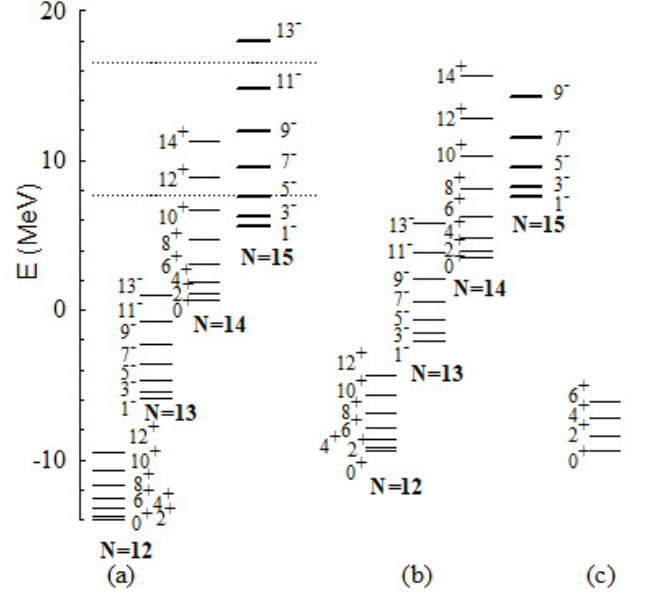


FIG. 5. Energy levels of  $^{48}\text{Ti}$  with respect to the  $\alpha$  threshold calculated with the potentials (a)  $V=181$  MeV and (b)  $V=171$  MeV are compared with (c) the experimental ground state band [66]. The energy levels are calculated in the bound state approximation except the  $N=15$  band resonances. The horizontal dotted lines indicate the incident energy  $E_\alpha = 8.4 - 18$  MeV of the fusion excitation functions in Fig. 3.

to the threshold anomaly [58]. With a decreased potential strength,  $V=171$  MeV (D171) with  $J_v = 367$  MeVfm<sup>3</sup>, the calculated ground band in Fig. 5(b) falls well in correspondence with the experimental ground band in Fig. 5(c). In Table II calculated rms intercluster radii and  $B(E2)$  values are given. The  $B(E2)$  values are calculated with the D171 potential and the  $L$ -dependent  $V$  tuned to reproduce the experimental excitation energy of the ground band because the  $L$ -dependence of  $V$  has been known widely, for example, in  $^{20}\text{Ne}$  [67],  $^{44}\text{Ti}$  [5, 6],  $^{94}\text{Mo}$  [68, 69],  $^{212}\text{Po}$  [68, 70] and  $^{46,50}\text{Cr}$  [71]. A small effective charge  $\Delta e = 0.1e$  is introduced for protons and neutrons. The experimental  $B(E2)$  values [72] are reproduced well. This small effective charge seems reasonable considering that core excitations are important in the  $^{44}\text{Ti}$  region [12, 73] and that the observed  $B(E2 : 2_1^+(1.157\text{MeV}) \rightarrow \text{g.s.})$  of  $^{44}\text{Ca}$ , 10.9 W.u., is large. The rms charge radius  $\langle r^2 \rangle^{1/2} = 3.71$  fm of the ground state calculated using the experimental values  $\langle r^2 \rangle_\alpha^{1/2} = 1.676$  fm and  $\langle r^2 \rangle_{^{44}\text{Ca}}^{1/2} = 3.518$  fm [74] is to be compared with the experimental value 3.59 fm [74]. The calculated intercluster distance of the ground state is about 85% of the sum of the experimental rms charge radii of the two clusters, which is only slightly small compared to 87% for the ground state of  $^{44}\text{Ti}$  [6]. For  $J = 0^+$ , the overlaps of the six deeply bound forbidden states supported by the potential with the harmonic oscillator wave functions with  $\hbar\omega = 10.41$  MeV, which is nearly equal to  $\hbar\omega = 10.5$  MeV used in the *ab initio* cal-



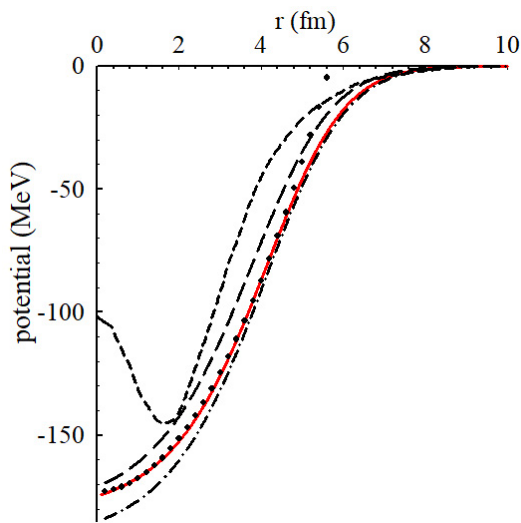


FIG. 6. (Color online) The D181  $\alpha+^{44}\text{Ca}$  potential at  $E_\alpha=18$  MeV (solid line) is compared with the Luneburg lens potential [44–46] with  $R_0=5.68$  fm and  $V_0=173$  MeV (points) and the energy-independent equivalent local potential for  $L=0$  in the GCM calculation [41] (medium dashed line). For comparison the  $\alpha+^{40}\text{Ca}$  potential used in the  $\alpha$  cluster calculation of  $^{44}\text{Ti}$  [6] (long dashed line) and the  $\alpha+^{48}\text{Ca}$  potential at  $E_\alpha=18$  MeV [15] (dashed-dot line) are also displayed.

culations of  $^{48}\text{Ti}$  in Ref. [75], are 1.000, 1.000, 0.999, 0.999, 0.996 and 0.977 for the oscillator quanta  $N_{HO}=0, 2, \dots, 10$ , respectively. This means that the obtained ground state wave function is orthogonal to the Pauli-forbidden states with  $N_{HO} \leq 10$  in the resonating group method mimicking Saito’s orthogonality condition model [76]. The probability with quanta  $N_{HO}$  component in the ground state wave function is 78.0, 11.3, 4.2, 1.8 and 1.0 % for  $N_{HO} = 12, 14, \dots, 20$ , respectively. The dominant  $N_{HO} = 12$  shell-model like component 78% is larger than that of  $^{44}\text{Ti}$  in Ref. [6]. The existence of the significant amount of higher  $N_{HO} \geq 14$  components, however, means that the ground state has  $\alpha$  clustering if modest. The  $2^+$  and  $4^+$  states have similar characters. This

means that  $\alpha$  clustering, i.e., sizable four-particle excitations from the  $fp$ -shell to the higher major shells, contributes not only to the large  $B(E2)$  values but also to the  $0\nu\beta\beta$  decay half-life of  $^{48}\text{Ca}$ , performing longer than the shell model within the  $N_{HO} = 12$  model space.

#### IV. DISCUSSION AND SUMMARY

In Fig. 6 the D181 potential is compared with a Luneburg lens [46] potential, which is a truncated harmonic oscillator potential [44, 45] given by  $V(r) = V_0 (r^2/R_0^2 - 1)$  for  $r \leq R_0$  and  $V(r) = 0$  for  $r > R_0$ . The potential resembles the Luneburg lens potential in the internal region, which explains why the potential embeds the deeply bound Pauli-forbidden states with  $N < 12$  and locates the Pauli-allowed  $N = 12$  band in correspondence to the experimental ground band. The energy dependence of  $J_v=388$  MeVfm<sup>3</sup> at 18 MeV and 356 MeVfm<sup>3</sup> at 24.1 MeV are consistently in line with  $J_v=340$  MeVfm<sup>3</sup> at  $E_\alpha=29$  MeV in Ref. [77]. The D181 potential in Fig. 6 is reasonable being in-between the potentials for  $\alpha+^{40}\text{Ca}$  and  $\alpha+^{48}\text{Ca}$ . The equivalent local potential of the microscopic GCM cluster model calculation[40, 41] belongs to a shallower potential family, which explains why the  $N=12$  band appears above the  $\alpha$  threshold energy and there appears no state corresponding to the ground state of  $^{48}\text{Ti}$ .

To summarize, the  $\alpha+^{44}\text{Ca}$  fusion excitation at  $E_\alpha=9-18$  was reproduced well by a global Luneburg lens-like potential, which fits  $\alpha+^{44}\text{Ca}$  scattering at  $E_\alpha=18-100$  MeV. The existence of a  $7^-$  state with the  $\alpha+^{44}\text{Ca}$  cluster structure of the higher nodal  $N=15$  band in  $^{48}\text{Ti}$  was confirmed for the first time at  $E_x = 18.8$  MeV in the bump of the fusion excitation function. The first Pauli-allowed  $N=12$  band with the  $\alpha+^{44}\text{Ca}$  cluster structure falls below the  $\alpha$  threshold in correspondence well with the experimental ground band of  $^{48}\text{Ti}$ . The experimental  $B(E2)$  values of the ground band were reproduced well by calculations and the enhancement is found to be due to  $\alpha$  clustering.

- 
- [1] K. Ikeda *et al.*, Prog. Theor. Phys. Suppl. No. **52**, 1 (1972) and references therein.
  - [2] K. Ikeda *et al.*, Prog. Theor. Phys. Suppl. No. **68**, 1 (1980) and references therein.
  - [3] S. Ohkubo, M. Fujiwara, and P. E. Hodgson, Prog. Theor. Phys. Suppl. **132**, 1 (1998) and references therein.
  - [4] S. Ohkubo, T. Yamaya, and P. E. Hodgson, Nuclear clusters, in *Nucleon-Hadron Many-Body Systems*, (edited by H. Ejiri and H. Toki) (Oxford University Press, Oxford, 1999), p. 150 and references therein.
  - [5] F. Michel, G. Reidemeister, and S. Ohkubo, Phys. Rev. Lett. **57**, 1215 (1986).
  - [6] F. Michel, G. Reidemeister, and S. Ohkubo, Phys. Rev. C **37**, 292 (1988).
  - [7] S. Ohkubo, Phys. Rev. C **38**, 2377 (1988).
  - [8] T. Yamaya, S. Oh-ami, M. Fujiwara, T. Itahashi, K. Katori, M. Tosaki, S. Kato, S. Hatori, and S. Ohkubo, Phys. Rev. C **42**, 1935 (1990).
  - [9] P. Guazzoni, M. Jaskola, L. Zetta, C. Y. Kim, T. Udagawa, and G. Bohlen, Nucl. Phys. **A564**, 425 (1993).
  - [10] T. Yamaya, K. Katori, M. Fujiwara, S. Kato, and S. Ohkubo, Prog. Theor. Phys. Suppl. **132**, 73 (1998).
  - [11] T. Sakuda and S. Ohkubo, Prog. Theor. Phys. Suppl. **132**, 103 (1998).
  - [12] S. Ohkubo, Y. Hirabayashi, and T. Sakuda, Phys. Rev. C **57**, 2760 (1998).
  - [13] F. Michel, S. Ohkubo, and G. Reidemeister, Prog. Theor. Phys. Suppl. **132**, 7 (1998).

- [14] M. Fukada, M. K. Takimoto, K. Ogino, and S. Ohkubo, Phys. Rev. C **80**, 064613 (2009).
- [15] S. Ohkubo, Phys. Rev. C **101**, 041301(R) (2020).
- [16] N. Anantaraman *et al.*, Phys. Rev. Lett. **35**, 1131 (1975).
- [17] H. W. Fulbright, C. L. Bennett, R. A. Lindgren, R. G. Markham, S. C. McGuire, G. C. Morrison, U. Strobusch, and J. Töke, Nucl. Phys. **A284**, 329 (1977).
- [18] T. A. Carey, P. G. Roos, N. S. Chant, A. Nadasen, and H. L. Chen, Phys. Rev. C **23**, 576 (1981).
- [19] T. A. Carey, P. G. Roos, N. S. Chant, A. Nadasen, and H. L. Chen, Phys. Rev. C **29**, 1273 (1984).
- [20] P. G. Roos, *Clustering Aspects of Nuclear Structure*, (edited by J. S. Lilley and M. A. Nagarajan) (D. Reidel Publishing Company, Dordrecht, 1985), p.279.
- [21] W. von Oertzen, Eur. Phys. J. A **11**, 403 (2001).
- [22] K. Tetsuno, S. Ajimura, K. Akutagawa, T. Batpurev *et al.*, J. Phys. Conf. Series **1468**, 012132 (2020).
- [23] J. D. Vergados, H. Ejiri, and F. Šimkovic, Rep. Prog. Phys. **75**, 106301 (2012).
- [24] J. Engel and J. Menéndez, Rep. Prog. Phys. **80**, 046301 (2017).
- [25] E. Caurier, J. Menéndez, F. Nowacki, and A. Poves, Phys. Rev. Lett. **100**, 052503 (2008).
- [26] M. Horoi, Phys. Rev. C **87**, 014320 (2013).
- [27] Y. Iwata, N. Shimizu, T. Otsuka, Y. Utsuno, J. Menéndez, M. Honma, and T. Abe, Phys. Rev. Lett. **116**, 112502 (2016).
- [28] L. Coraggio, A. Gargano, N. Itaco, R. Mancino, and F. Nowacki, Phys. Rev. C **101**, 044315 (2020).
- [29] J. M. Yao, B. Bally, J. Engel, R. Wirth, T. R. Rodríguez, and H. Hergert, Phys. Rev. Lett. **124**, 232501 (2020).
- [30] A. Belley, C. G. Payne, S. R. Stroberg, T. Miyagi, and J. D. Holt, Phys. Rev. Lett. **126**, 042502 (2021).
- [31] F. Šimkovic, V. Rodin, A. Faessler, and P. Vogel, Phys. Rev. C **87**, 045501 (2013).
- [32] J. Hyvärinen and J. Suhonen, Phys. Rev. C **91**, 054308 (2015).
- [33] J. Terasaki, Phys. Rev. C **91**, 034318 (2015).
- [34] P. K. Rath, R. Chandra, K. Chaturvedi, P. K. Raina, and J. G. Hirsch, Phys. Rev. C **82**, 064310 (2010).
- [35] T. R. Rodriguez and G. Martinez-Pinedo, Phys. Rev. Lett. **105**, 252503 (2010).
- [36] N. Hinohara and J. Engel, Phys. Rev. C **90**, 031301(R) (2014).
- [37] N. L. Vaquero, T. R. Rodríguez, and J. L. Egido, Phys. Rev. Lett. **111**, 142501 (2013).
- [38] J. M. Yao, L. S. Song, K. Hagino, P. Ring, and J. Meng, Phys. Rev. C **91**, 024316 (2015).
- [39] J. Barea and F. Iachello, Phys. Rev. C **79**, 044301 (2009); J. Barea, J. Kotila, and F. Iachello, Phys. Rev. Lett. **109**, 042501 (2012).
- [40] K. Langanke, Nucl. Phys. **A377**, 53 (1982).
- [41] D. Wintgen, H. Friedrich, and K. Langanke, Nucl. Phys. **A408**, 239 (1983).
- [42] S. Bailey, T. Kokalova, M. Freer, C. Wheldon, R. Smith, J. Walshe *et al.*, Eur. Phys. J. A **57**, 108 (2021).
- [43] S. Bailey, T. Kokalova, M. Freer, C. Wheldon, R. Smith, J. Walshe *et al.*, Phys. Rev. C **100**, 051302(R) (2019).
- [44] F. Michel, G. Reidemeister, and S. Ohkubo, Phys. Rev. Lett. **89**, 152701 (2002).
- [45] S. Ohkubo, Phys. Rev. C **93**, 041303(R) (2016).
- [46] R. K. Luneburg, *Mathematical Theory of Optics* (University of California Press, Oakland, California, 1964).
- [47] A. Budzanowski, K. Grotowski, L. Jarczyk, B. Lazarka, S. Micik, H. Niewodniczański, A. Strzałkowski, and Mrs. Z. Wróbel, Phys. Lett. **16**, 135 (1965).
- [48] C. R. Gruhn and N. S. Wall, Nucl. Phys. **81**, 161 (1966).
- [49] G. Gaul, H. Lüdecke, R. Santo, H. Schmeing, and R. Stock, Nucl. Phys. **A137**, 177 (1969).
- [50] Th. Delbar, Gh. Grégoire, G. Paic, R. Ceuleneer, F. Michel, R. Vanderpoorten *et al.*, Phys. Rev. C **18**, 1237 (1978).
- [51] J. Albiński and F. Michel, Phys. Rev. C **25**, 213 (1982).
- [52] D. M. Brink, *Semi-Classical Methods for Nucleus-Nucleus Scattering* (Cambridge University Press, Cambridge, U.K., 1985).
- [53] F. Michel, G. Reidemeister, and S. Ohkubo, Phys. Rev. C **34**, 1248 (1986).
- [54] K. A. Eberhard, C. Appel, R. Bangert, L. Cleemann, J. Eberth, and V. Zobel, Phys. Rev. Lett. **43**, 107 (1979).
- [55] S. Ohkubo and D. M. Brink, Phys. Rev. C **36**, 966 (1987).
- [56] S. Ohkubo and D. M. Brink, Phys. Rev. C **36**, 1375 (1987).
- [57] U. Mosel, in *Treatise on Heavy Ion Science*, edited by D. A. Bromley, (Plenum, New York, 1984), p.3 and see references therein.
- [58] C. Mahaux, H. Ngo, and G. R. Satchler, Nucl. Phys. **A449**, 354 (1986); C. Mahaux, H. Ngo, and G. R. Satchler, **A456**, 134 (1986).
- [59] P. Swan, Proc. R. Soc. A **228**, 10 (1955).
- [60] C. Beck, A. M. Mukhamedzhanov, and X. Tang, Eur. Phys. J. A **56**, 87 (2020).
- [61] C. L. Jiang, B. B. Back, K. E. Rehm, K. Hagino, G. Montagnoli, and A. M. Stefanini, Eur. Phys. J. A **57**, 235 (2021) and references therein.
- [62] F. Nemoto and H. Bando, Prog. Theor. Phys. **47**, 1210 (1972).
- [63] J. Hiura, F. Nemoto, and H. Bando, Prog. Theor. Phys. Suppl. **52**, 173 (1972).
- [64] S. Ohkubo, Y. Kondo, and S. Nagata, Prog. Theor. Phys. **57**, 82 (1977).
- [65] Y. Fujiwara, H. Horiuchi, K. Ikeda, M. Kamimura, K. Kato, Y. Suzuki, and E. Uegaki, Prog. Theor. Phys. Suppl. **68**, 29 (1980) and references therein.
- [66] T. W. Burrows, Nucl. Data Sheets **107**, 1747 (2006).
- [67] F. Michel, Y. Kondo, and G. Reidemeister, Phys. Lett. **B 220**, 479 (1989).
- [68] S. Ohkubo, Phys. Rev. Lett. **74**, 2176 (1995).
- [69] M. A. Souza and H. Miyake, Phys. Rev. C **91**, 034320 (2015).
- [70] D. Ni and Z. Ren, Phys. Rev. C **83**, 014310 (2011).
- [71] P. Mohr, Eur. Phys. J. A **53**, 209 (2017).
- [72] R. Ernst *et al.*, Phys. Rev. Lett. **84**, 416 (2000); R. Ernst *et al.*, Phys. Rev. C **62**, 024305 (2000).
- [73] K. Arnsward *et al.*, Phys. Lett. B **772**, 599 (2017).
- [74] I. Angeli and K. P. Marinova, Atomic Data and Nucl. Data Tables **99**, 69 (2013).
- [75] J. P. Vary, S. Popescu, S. Stoica, and P. Navrátil, J. Phys. G Nucl. Part. Phys. **36**, 085103 (2009).
- [76] S. Saito, Prog. Theor. Phys. **40**, 893 (1968); S. Saito, Prog. Theor. Phys. **41**, 705 (1969).
- [77] F. Michel and R. Vanderpoorten, Phys. Lett. **82 B**, 183 (1979).